

A NEW APPROACH FOR URBAN ROADS DETECTION USING LASER DATA AND AERIAL DIGITAL IMAGES

Anderson A. Gohara¹, Mário A. Pazoti^{1*}, Francisco A. Silva¹, Danillo R. Pereira¹,
Almir O. Artero² and Marco A. Piteri²

¹ *Department of Computer Science, University of Western São Paulo (Unoeste), Presidente Prudente,
São Paulo, Brazil*

² *Faculty of Science and Technology, São Paulo State University (Unesp)
Presidente Prudente, São Paulo, Brazil*

Received 21 July 2015; received in revised form 01 June 2016; accepted 10 June 2016

Abstract:

The automatic feature extraction from digital aerial images is not a trivial task mainly due to occlusion problems, shadows and different viewpoints. To obtain an improved feature extraction we used laser data, which have additional information such as height and material type of the surface. In this paper we performed the combination of digital image and laser data in order to improve the results of automatic extraction of urban roads. Initially, the urban roads were detected from the response of laser information; in the sequence we applied two different approaches to connect the disconnected road segments. The results were very promising, with sensitivity rate of 92%.

Keywords: Digital Terrain Model; Urban Roads; Laser Data; Feature Detection

© 2016 Journal of Urban and Environmental Engineering (JUEE). All rights reserved.

* Correspondence to: Mário A. Pazoti, Tel.: +55 18 3229 1060.
E-mail: mario@unoeste.br

1 INTRODUCTION

Feature extraction is a very pursued problem that has received considerable attention in the last decade. The extraction of rural road network is a topic widely researched, however, the extraction of road network in dense urban areas is a very hard task and there are few works related to theme (Baumgartner *et al.*, 1999). The factors that make difficult this process are the heterogeneity of the objects in the image, and the relationship between roads and buildings, trees, cars, etc. This complexity is also inherent in the extraction process of other urban features, such as the contours of roofs, house identification and etc. This context shows that the extraction of urban objects can lead to obstacles very hard to overcome (Galvanin & Dal Poz, 2009).

The extraction of cartographic features can be divided into two steps, they are (i) recognition, and (ii) delineation. Both tasks are performed by automated or semi-automated methods. Although semi-automatic methods depend on the assistance of an operator, they perform all the delineation task of tracing features, which is usually time consuming and onerous (Dal Poz *et al.*, 2006; Mena, 2003).

High resolution images provide detailed spatial information of the earth's surface such that urban the features are represented by pixels and used in many extraction methods. However, this information can be insufficient for the classification of urban land coverage. Existing occlusions can cause loss of spectral information in some images (Araki, 2005). The classification by points considering only the height is also not enough to identify objects such as buildings, due to noise and small differences in height of between neighbor sampling points (Centeno & Mitishita, 2007). These problems can be overcome combining the laser data (which contains altimetry information about the surface) and digital images (containing color information), thus improving the discrimination of coverage. An important point is that for the merging data from different sources (such as cartographic bases, altimetry data and images) are necessary the spatial references be the same (Araki, 2005).

In this paper we presented a novel algorithm that combines the digital image and laser data for automatic extraction of urban roads; that facilitate the extraction of urban roads that is often manually executed by cartographers. Therefore, the main contribution of this paper is to propose an automated approach for extraction of urban roads. Additionally, the proposed methodology can be employed in others applications of feature extraction.

The remaining of this paper is organized as follow. In Section 2 the laser scanning process is detailed. The process of generation of the regular grid of points is presented in Section 3. In Section 4 focuses about roads extraction, with and without the use of laser data. The proposed algorithm used to generate a Digital Terrain

Model is introduced in Section 5. In Section 6 the procedures used in each stage of urban roads extraction are detailed. The detailed analyses of the results are performed in Section 7. Lastly, in Section 8 is presented our conclusions and proposals for future work.

2 LASER SCANNING PROCESS

Currently, the seeks technologies that enable greater speed and accuracy in delivering results is very pursued. One of these technologies that have been commonly used in photogrammetry is the data from the laser scanning system, which can be of two types: (i) static or (ii) dynamic. The static surface mapping scanning is performed from a fixed point; differently, the dynamic surface mapping scanning is done from a mobile platform (Wutke, 2006).

The laser scanning system named Lidar (Light Detection and Ranging) or Ladar (Laser Detection Ranging) is a technology designed for measuring three-dimensional coordinates of a point on a surface. This system is based on the emission of a laser pulse (Centeno & Mitishita, 2007).

The basic operation of the laser scanning system consists of sending a laser pulse toward a target surface, capturing the reflection on the hit surface. The process of laser scanning is classified into two class, they are: (i) triangulation and (ii) "time-of-light" (Centeno & Mitishita, 2007).

Systems that operate on the triangulation principle use a laser transmitter and a camera to capture the laser data. According to the distance between the hit surface and the sensor, the reflection of laser pulse appears at different points on the camera image plane. A triangle is formed by the issuer, the camera and the point on the hit surface (Centeno & Mitishita, 2007). Based on this triangulation is possible to calculate the distance between the scanning system and the hit surface. In **Fig. 1** is illustrated a configuration of two laser pulses of different positions on the image plane camera.

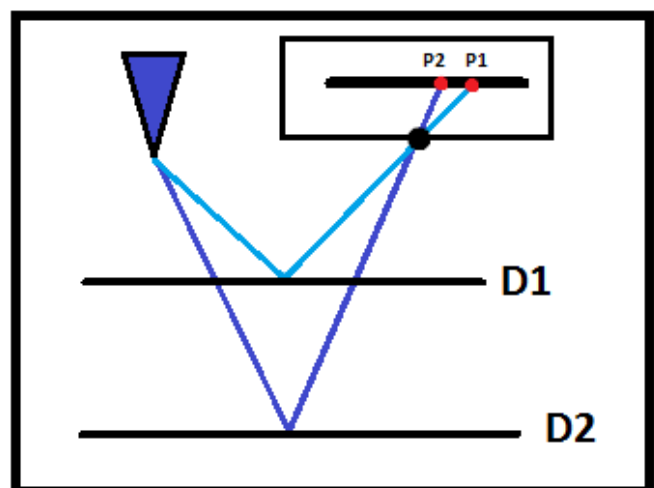


Fig. 1 Triangulation performed by laser system for different distances of two different points.

Systems that operate on the time-of-flight principle are based on the time past from the emission of the laser pulse and its return (reflection). **Equation (1)** shows the distance computation formula:

$$R = c \cdot dt / 2 \quad (1)$$

where R is the distance between the hit surface and the laser scanning system, c is the propagation speed of a laser beam and dt is the time past from the emission and reception of the laser pulse.

A set of 3D points on a surface that is generated by a laser scanning is called Digital Elevation Model (DEM). During the scanning process, the points of different surfaces can be collected, as: buildings, trees, cars, etc. (Centeno & Mitishita, 2007). It is interesting noting that Digital Elevation Models (DEM) and Digital Terrain Models (DTM) are different models. Both models are formed by a set of points over a surface, however in DEM the points denote all the elevation of the surface (including buildings, trees, cars, etc.); differently, in DTM the points represent only the ground characteristics, such as soil, water etc. (Fazan & Dal Poz, 2013). The DTMs are widely applied in the generation of orthophotos and topographic maps, as well in the study of soil characteristics.

3 GRID GENERATION

The set of points provided by the laser scanning system is named cloud of points, which contains a set of three-dimensional coordinates irregularly distributed. As our approach uses digital image processing techniques, then it became necessary to define a regular grid G in cloud to the points.

Initially, we defined a dimension size n of the regular grid over the set of points that determines the spacing in the X and Y axes. Then, all coordinates x_i and y_i have associated a z_i coordinate and the intensity value I (intensity of laser pulse response) that are obtained by the average of the values in the cell, as shown in **Eqs (2)** and **(3)**.

$$z_i = \frac{\sum_{j=1}^n z_{ij}}{n} \quad (2)$$

$$I_i = \frac{\sum_{j=1}^n I_{ij}}{n} \quad (3)$$

In order to determine the grid dimension, we computed the average X and Y distance between each pair of adjacent points. Both set were sorted and had distinct values. **Equations (4)** and **(5)** show the process of computation.

$$u_x = \frac{\sum_{i=1}^n |x_i - x_{i+1}|}{n} \quad (4)$$

$$u_y = \frac{\sum_{i=1}^n |y_i - y_{i+1}|}{n} \quad (5)$$

Lastly, we defined d_x and d_y values that denotes the X and Y dimension of the grid. **Equations (6)** and **(7)** show the formulation to determine the final dimensions of the grid.

$$d_x = \frac{|x_{\max} - x_{\min}|}{u_x} \quad (6)$$

$$d_y = \frac{|y_{\max} - y_{\min}|}{u_y} \quad (7)$$

where x_{\max} and x_{\min} represents the maximum and the minimum of the coordinates x_i ; analogously, y_{\max} and y_{\min} denotes the maximum and the minimum of the coordinates y_i .

4 RELATED RESEARCHES

The literature presents various techniques, methodologies and algorithms related to the road extraction in orbital and flight images, with and without the use of laser data. Some of these methods are presented below.

For example, Silva (2003) presented a method for detection and automatic rebuilding of road joins in digital images of rural areas. This method requires the road segments be previously extracted through a semi-automatic method. The method is based on two steps:

(1) Potential areas of highway junctions are detected through the criteria of proximity and radiometric homogeneity. The proximity criterion detects clusters of points belonging to the highway segments that are distant from each other at maximum distance. The criterion of radiometric homogeneity checks if the region bounded by points detected by the first criterion is radiometrically consistent with the road bed. The points of groups that satisfy this criterion are accepted as belonging to the highway junctions.

(2) Four highway junction models are used to represent the typical forms of joint occurrence in images of rural scenes. These models allow the reconstruction of joints found in the previous step. The road junction reconstruction process consists in calculating the most representative point of the geometrical center of the junction region and establishing connections between this point and the junction region of the points detected in the previous method step.

Mendes *et al.* (2004) present a method for the design of local roads in digital images, performing a combination of a linear extrapolation technique, and a highway delineator based on correlation techniques. A highway axis point, previously extracted, is linearly extrapolated, resulting in an approximate position.

This position is refined by the highway delineator based on the correlation among grayscale profiles,

extracted transversely to the highway axis. This strategy is repeated until the delineation of the entire axis of the road.

Alves (2007) evaluated the semi-automatic extraction of roads on the extract of a hybrid image, aiming to apply this in the cartography. The results obtained by the algorithm based on dynamic programming ('ERGeo') were compared with the results of photo-interpretation and a field survey (taken as reference). For this, it was used a rural area of a cartographic base 1:50 000 from the City of Silva Jardim, RJ Brazil. The scenes (images) obtained by CBERS and SPOT satellites were combined through the merger by principal components and the processing of images were performed to increase the contrast and highlight the road features.

Other related works merge different types of information. Araki (2005) presents a method to merge altimetry and spectral information data and auxiliary data in the high resolution image classification. The spectral information is presented in high-resolution images, although represent the earth's surface in detail, the information are insufficient for urban land cover classification. This is due to loss of information by occlusion. This problem can be solved by using altimetry data acquired by airborne system, improving discrimination. Another possibility is the use of auxiliary information present in cartographic bases in order to assist the discrimination of classes. An important point for merging data from these different sources is the need of a common spatial reference. The method for classification has to handle data corresponding to scales of numerical and nominal measurements, and does not depend on the assignment of a particular statistical distribution for classes. Decision trees, OPF and SVM (Pereira & Nakamura, 2015) are an alternative for the supervised classification, however this methods demands a ground-truth for the training step.

There are researches that use laser data for the extraction of roads. Castro *et al.* (2009) presents a methodology for road extraction from laser intensity images using mathematical morphology. The roads are features on maps, which can be highlighted for its dynamism due the modifications in its shape or texture, type - paved or unpaved - and/or inclusion of new roads or stretches on the road system. The first step is to generate a DTM from the height data. Then the roads are classified according to the expected range for the intensity of the laser pulse and for the height difference in a neighbourhood.

Hu *et al.* (2004) combine laser data and aerial images. The recognition of roads from aerial images can be supplemented by using the laser data to detect shaded areas not captured by the image, facilitating the extraction.

5 GENERATING DIGITAL TERRAIN MODEL

A resource used in one of the stages of this study is the Digital Terrain Model (DTM). DTM is a 3D mapping of the land, excluding all objects on its surface such as house, buildings, cars, and more. The DTM cannot be generated directly from the laser scanning system. Thus, it was generated by filtering the Digital Elevation Model (DEM).

The chosen filter is the proposed by Vosselman (2000), in this filter is defined a function $\Delta h_{max}(d)$ where the maximum height grows proportionally to the distance d . The idea of the filter is to exclude all points that not belong to the terrain. It is performed at a specific direction, based on the inclination of the terrain, as shown in **Fig 2** and **3**.

The first step of this filter is to detect the first points outside the ground. It is necessary to know the region of interest that is determined by the adjacent points to the initial points. The two procedures that classify a point as belonging or not to the terrain are shown in **Algorithm 1** and **Algorithm 2**. **Algorithm 1** receives as parameter a set A of adjacent points, an initial point p , and a maximum height defined by $hmax = \Delta h_{max}(d)$. In the algorithm is verified whether exists a point among the elements of A that has a height difference bigger than $hmax$. In **Algorithm 2** it is done the opposite process.

Algorithm 1 Detection of points that do not belong to the set.

```
DetectPointNotBelonging ( A , p, hmax )
  i ← 0
  while i < size[A] do
    h ← p.h - A[i].h
    if h > hmax then
      return TRUE
    i ← i + 1
  return FALSE
```

Algorithm 2 Detection of points that belong to the set.

```
DetectPointBelonging ( A , p, hmax )
  i ← 0
  while i < size[A] do
    h ← p.h - A[i].h
    if h <= hmax then
      return TRUE
    i ← i + 1
  return FALSE
```

If the declivity of the region analyzed is insignificant, it is possible that the point of continuity that should be detected by **Algorithm 2**, never is found or it is found too far; causing errors. For this reason, the algorithm has a propagation limit that in case no continuity point is found in the distance limit, no point is removed from that region.

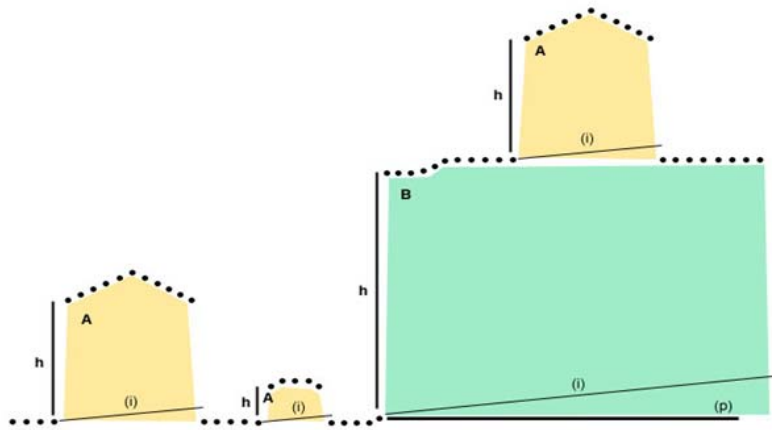


Fig. 2 Example of filtering; (i) possible inclination line of the terrain based on a starting point on the terrain; (p) limit propagation line of the inclination rule, starting from the beginning of the inclination line; (A) objects on the terrain, as houses, cars, etc.; (B) Natural relief area, as valleys and mountains for example; (h) height difference between two points.

Algorithm 3 Filtering of points that do not belong to the terrain.

```

Filtering ( G, hmax, prop )
  create G'
  width[G'] ← width[G]
  height[G'] ← height[G]
  for i ← 0 until width[G] do
    for j ← 0 until height[G] - 1 do
      A' ← { G[i][j + 1] }
      if DetectPointNotBelonging (A', G[i][j], hmax) do
        j ← j + 1
        A' ← { G[i][j+1] }
        c ← 0
        j' ← j - 1
        while j < height[G] - 1 and c < prop and
          DetectPointNotBelonging (A', G[i][j], hmax) do
          j ← j + 1
          A' ← { G[i][j+1] }
        j ← j - 1
        if c = prop then
          j ← j'
      else
        G'[i][j] ← G[i][j]
    j ← j + 1
  i ← i + 1
return G'
    
```

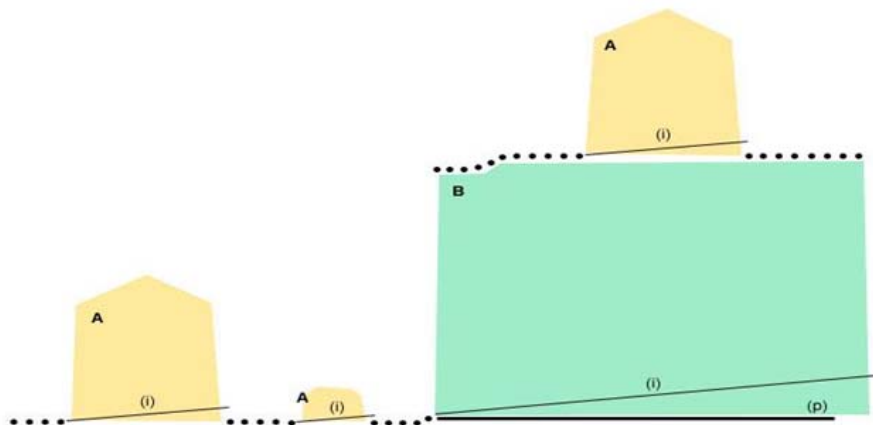


Fig. 3 Example of a filtered area after points from region A were removed; (i) possible inclination line of the terrain, based on a starting point on the terrain; (p) limit propagation line of the inclination rule, starting from the beginning of the inclination line; (A) objects on the terrain, as houses, cars, etc.; (B) Natural relief area, as valleys and mountains for example.

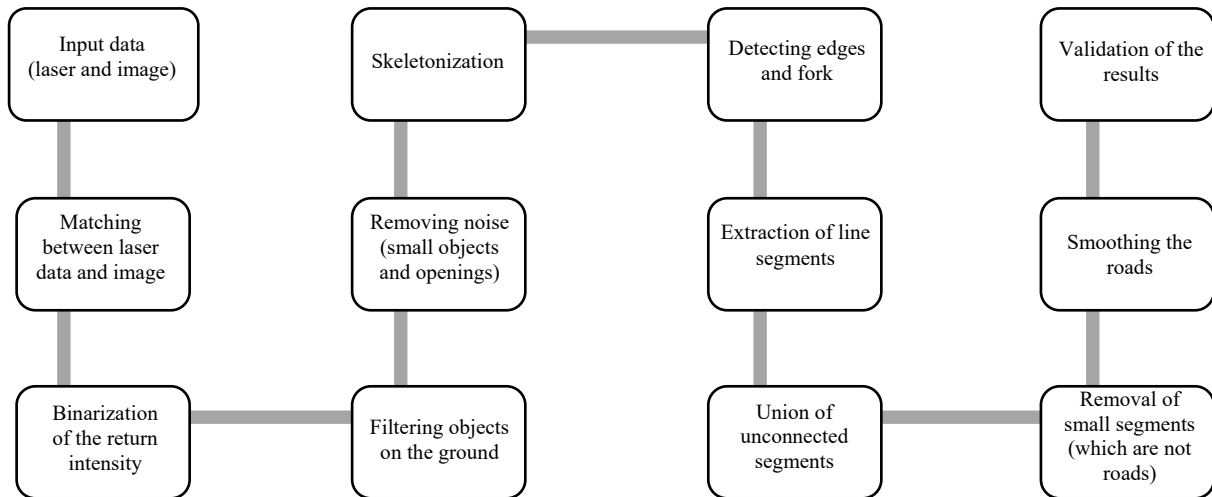


Fig. 4 Process flowchart of the urban roads extraction.

This way, if the propagation exceeds the propagation limit, the searching process defined in **Algorithm 1** is continued from the following state. In **Algorithm 3** is shown the algorithm of the filtering process in the vertical direction. After the filtering process, the points that do not belong to the terrain are excluded. In **Fig. 2** and **Fig. 3** are illustrated the filtering method, where points from A (objects) are eliminated and points from B (natural relief) are preserved.

6 ALGORITHM FOR URBAN ROADS EXTRACTION

In this section we presented a new algorithm based on computer vision techniques for the extraction of urban roads using as input the laser data and digital aerial images.

6.1 Steps

The proposed algorithm can be seen as a schematic diagram that is represented by the flowchart of **Fig. 4**.

6.1.1 Matching Between Laser Data and Digital Image

Differences in scale, density and angulation, results in the lack of a direct match between a point in the DEM matrix and the same point on the digital image, due the fact that no prior treatment was performed in the laser data or images for this purpose. In this work we use color, altitude and surface material information to carry out matching between these data.

Matching between high resolution images and laser data was performed by manually selecting common points between the digital image and greyscale image generated from laser data, as illustrated in **Fig. 5**. After defining the set of points, we calculated a transformation matrix that represents the mapping



Fig. 5 Selection of common points between the image generated from the laser data (a) and the high resolution image (b) to perform matching.

between laser data and aerial image. This matrix is formed by the accumulation of two geometric transformation matrices: scale and rotating. The scale matrix S_{xy} is calculated by the distance between the selected points, while the rotation matrix $R(\theta)$ is calculated by the angle θ between vectors formed by points. The matrix composition is shown in **Equations (8)** and **(9)**. The next step is the association of each point of the high resolution image with its respective point in the DEM and vice versa.

$$M = R(\theta).S_{xy} \tag{8}$$

$$M = \begin{bmatrix} \cos(\theta) & -\sin(\theta) & 0 \\ \sin(\theta) & \cos(\theta) & 0 \\ 0 & 0 & 1 \end{bmatrix} \begin{bmatrix} S_x & 0 & 0 \\ 0 & S_y & 0 \\ 0 & 0 & 1 \end{bmatrix} \tag{9}$$

Due to differences in resolution between the two data sources it was necessary to perform an adjustment in the mapping of the digital image to the DEM. Thus, it is assured that every pixel in the digital image is mapped to the corresponding point in the laser data, except where there is no corresponding point.

6.1.2 Laser Data Filtration

The laser data contains two types of information, they are: (i) the altimetry that represents the surface height; and (ii) the response intensity, which represents the surface material. In this work, we use both information to extract roads. First, we generated a binarized image from the response intensity data, where the darker points correspond to low response intensity and the brighter points correspond to higher response intensity, as shown in **Fig. 6**.

The asphalt is a specific type of material that has very low response intensity, as shown in **Table 1**. Then we removed all points whose response intensity is higher than this threshold. The result of this step is shown in **Fig. 7**.

It is possible to see that most of the road remained in the binarized image; however, there are many of noise. In order to reduce noise we applied two simple filters that remove surfaces higher than terrain and eliminate regions that are considered small. The filters are exemplified in the following subsections.

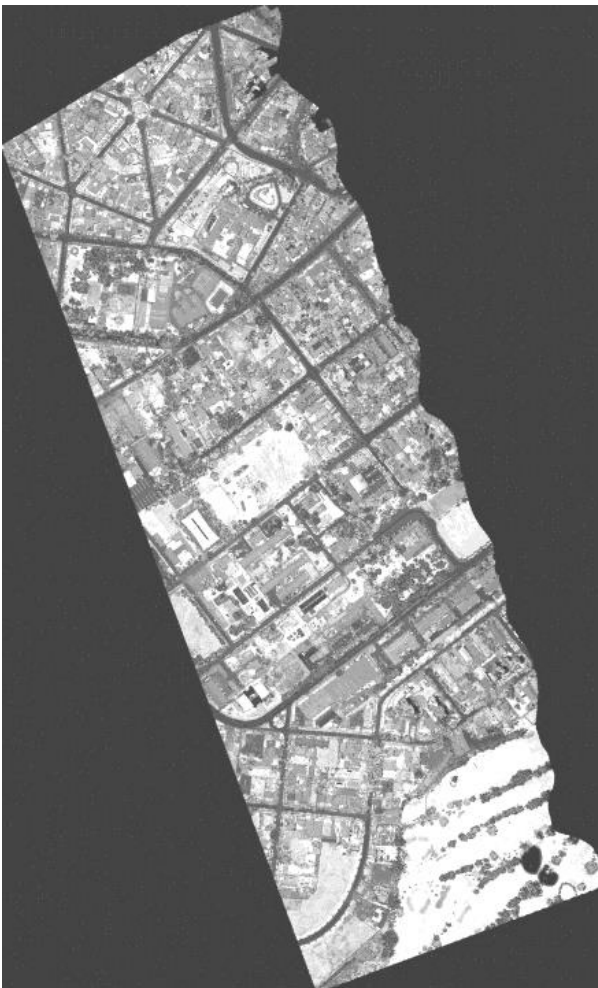


Fig. 6 Image generated from response intensity of laser data.

Table 1. Percentage of response intensity for some type of materials (Galvanin & Dal Poz, 2009)

Material	Reflection (%)
Clear, dry and clean wood	94
Snow	80–90
Bright stones	85
Clay, limestone	until 75
Miscellaneous vegetation	60
Conifers	30
Asphalt	17

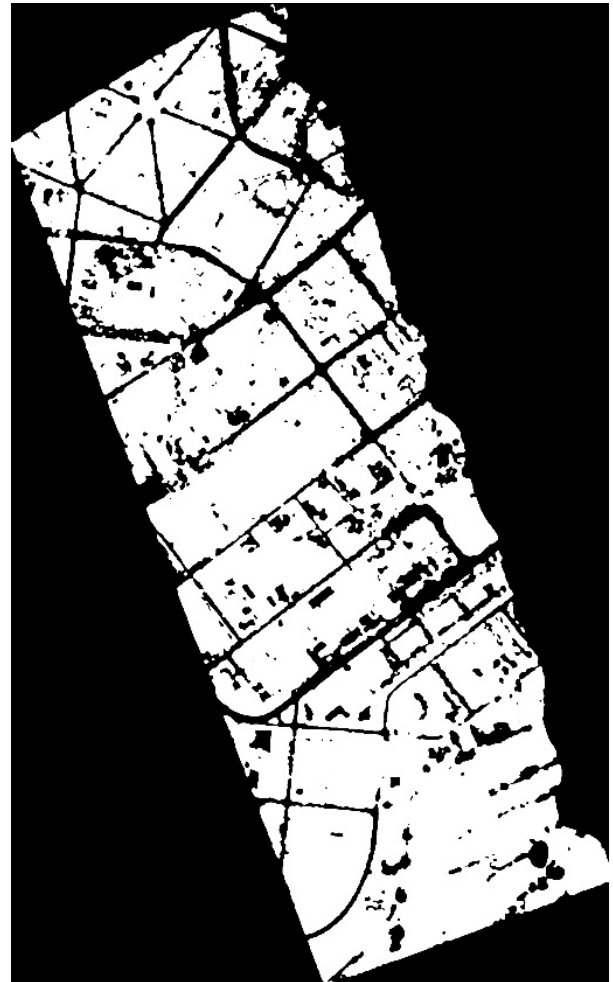


Fig. 7 Binarized response intensity image.

6.1.3 Removal of objects higher than terrain

We consider that roads are soil regions covered by asphalt. Thus, urban roads cannot be higher than terrain level. Then, regions higher than terrain level were removed; it was performed using the DTM and DEM. All points in the DEM with a higher value for the Z coordinate is considered to be above the terrain and must be removed.

This step was useful to remove objects with low response intensity material, but higher than terrain level. The result is of this filtering process is shown in **Fig. 8**.

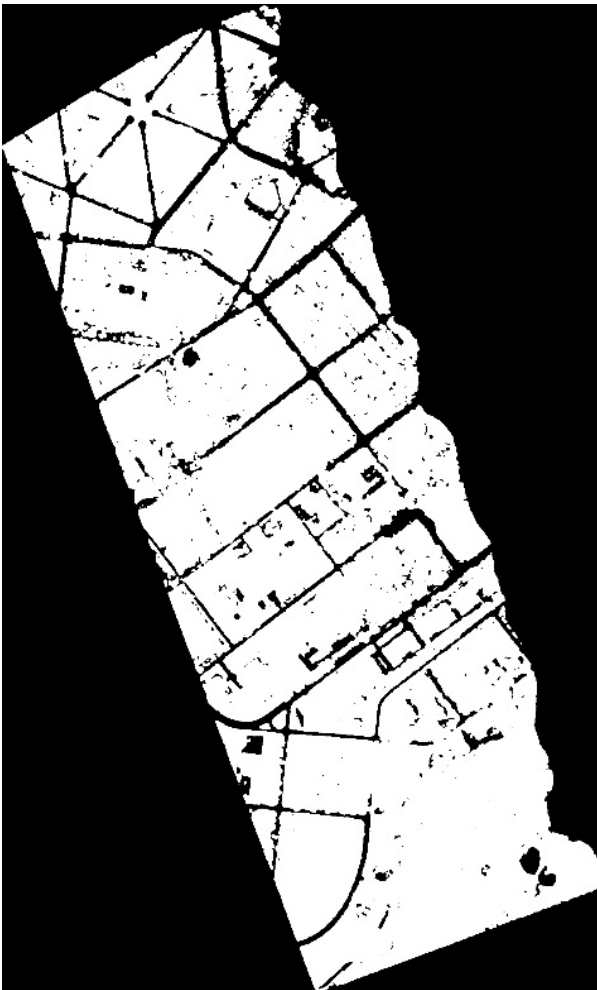


Fig. 8 Result of removal of points higher than terrain level.



Fig. 9 Image after being eroded and dilated.

6.1.4 Noise Removal

We removed noise from the images using the two mathematical morphology operations: (i) erosion and (ii) dilation. This process removes small noises and highlights important parts, as shown in Fig. 9.

6.1.5 Removal of Small Objects

Commonly, images have a large size on least one dimension, i.e., even though they are narrow, they have an elongated shape. This characteristic facilitated the removal of small objects. In order to perform this step we used the Flood Fill algorithm in two steps. In the first step is defined the size of the objects. The size was calculated from the distance between P1 (X_{min}, Y_{min}) and P2 (X_{max}, Y_{max}). The calculation of the Euclidian distance is shown in Eq. (10). The distance between P1 and P2 correspond the length of the diagonal of the bounding box of the object, as shown in Fig. 10. The result of this filtering process is shown in Fig. 11.

$$D = \sqrt{(X_{max} - X_{min})^2 + (Y_{max} - Y_{min})^2} \quad (10)$$

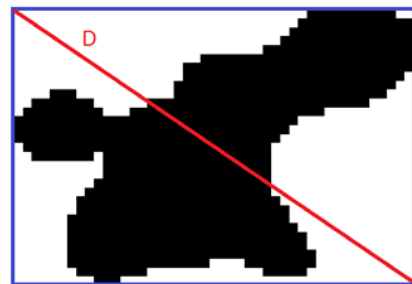


Fig. 10 Bounding box and diagonal length of an object.

6.1.6 Skeletonization

From the result of the filtering and binarization applied to the laser data we generated a skeleton. The skeletonization algorithm used was the one proposed by Zhang & Suen (1984). The algorithm considers only pixels that have 8 neighbors, i.e., bordering pixels are not considered. For each pixel P1 to be analyzed, we compute A(P1) and B(P1). A(P1) is the number of transitions from white to black running through the neighbors of P1 in the following sequence P2, P3, P4, P5, P6, P7, P8, P9, P2. The neighbors are determined as shown in Fig. 12. B(P1) is the number of black neighbors of P1. The algorithm consists of two parts:

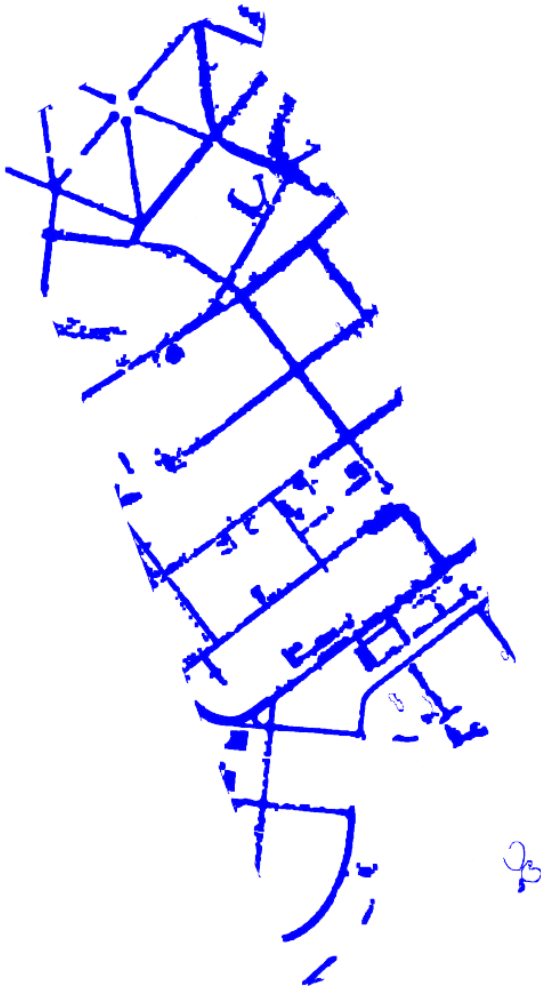


Fig. 11 Small objects are removed according the size.

P9	P2	P3
P8	P1	P4
P7	P6	P5

Fig. 12 Neighbors of P1 determined for skeletonization.

In the first step all pixels are tested to verify which satisfy all the following conditions:

- It is black and has 8 neighbors
- $2 \leq B(P1) \leq 6$
- $A(P1) = 1$
- At least one among P2, P4 and P6 is white.
- At least one among P4, P6 and P8 is white.

The pixels that satisfy simultaneously all the conditions are defined as white.

In the second step, all pixels are tested to verify if satisfy all the follow conditions:

- It is black and has 8 neighbors.
- $2 \leq B(P1) \leq 6$
- $A(P1) = 1$

- At least one among P2, P4 and P8 is white.
- At least one among P2, P6 and P8 is white.

The pixels that satisfy simultaneously all previous conditions are define as white. The steps 1 and 2 are repeated until no point is modified in any of the two steps. The result of the skeletonization is shown in Fig. 13.

From the skeleton we extracted keypoints as extremities and fork. A point in the skeleton is considered an extremity if the pixel that represents it belongs to the skeleton and has exactly one neighbor that also belongs to the skeleton, as exemplified in Fig. 14.

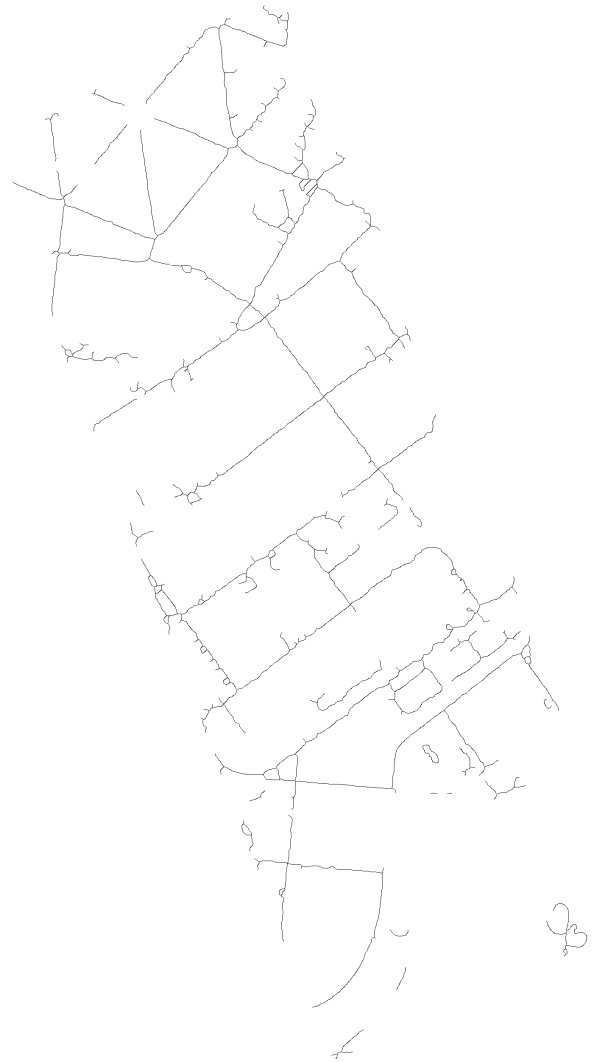


Fig. 13 The output image of skeletonization process.



Fig. 14 Detected extremities are colored in red.

One point is considered a fork if from the point, the line is separated in two or more lines, or if the point represents the intersection of two or more lines, as exemplified **Fig. 15**.

To verify if a pixel represents a bifurcation, we have to compute the number of neighbor pixels that belong to the skeleton. The pixel is considered a bifurcation if it has more than two neighbors that belong to the skeleton.

For counting the neighbors, we first consider the neighbors of the Four-neighbor rule, i.e., the upper neighbor, the lower neighbor, the left neighbor and the right neighbor, represented by P1, P2, P3 and P4, respectively (**Fig. 16**). The neighbors of the diagonals P12, P23, P34 and P41 are only considered if the adjacent Four-neighbor pixels do not belong to the skeleton. For example, the point P12 is verified only if the points P1 and P2 do not belong to the skeleton. Similarly, the point P23 is verified only if the points P2 and P3 do not belong to the skeleton. The same process is performed for P23 and P41.

The counting is executed this way to avoid that some specific points are misclassified as a bifurcation; given the fact that some points have more than two neighbors and they are not bifurcations. In **Fig. 17** we have a pixel (represented by the red square) that despite having 4 neighbors (represented by the blue squares) and it is not a bifurcation.



Fig. 15 Example of a detected bifurcation.

P41	P1	P12
P4	P	P2
P34	P3	P23

Fig. 16 Neighbors of the pixel P1.

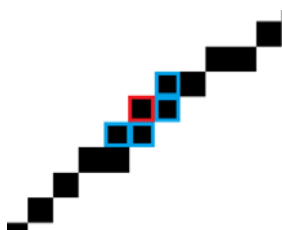


Fig. 17 Example of degenerate neighborhood.

6.1.7 Segments

From the points of bifurcation and extremities, the skeleton is divided into segments. Each segment corresponds to a sequence of continuous pixels from a bifurcation or an extremity to the next bifurcation or extremity, as shown in **Fig. 18**. Those segments are used to reconstruct the roads

6.1.8 Segments linking

These segments represent possible roads. In some cases, part of a road is not detected and the segments can contain discontinuities. However, a road should be represented by a continuous segment of pixels defined by two or more smaller segments. To overcome this problem, we connect segments with discontinuities, as shown in **Fig. 19**.

The segments connections are realized in two steps. The first step consists in rules based in angulation and distance. The threshold for angulation and distance were defined empirically. The distance is determined by the Euclidian distance, shown in **Eq. (9)**, between the extremities of each segment. This distance should be smaller than the threshold determined by the rule. To compute the angle we defined three vectors, one for each segment and one for the new segment that will be generated. For example, in **Fig. 20** we have vectors $V1=(a1,a2)$ representing the segment *A*, $V2=(b1, b2)$ representing the segment *B* and $V3=(a2,b1)$ representing the possible link between the segments *A* and *B*. The angle between *V1* and *V2* and the angle between *V1* and *V3* are computed. These angles have to be smaller than the threshold established by the rule. The angle α between two vectors *u* and *v* is computed by **Eq. (11)**.

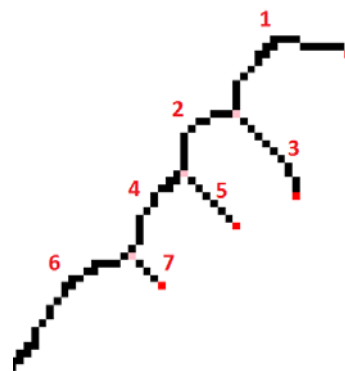


Fig. 18 Part of a skeleton divided in 6 segments defined by bifurcations and extremities.

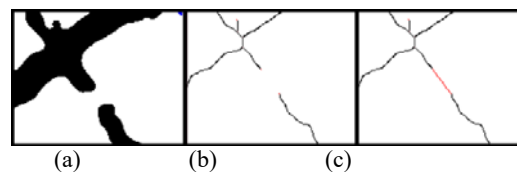


Fig. 19 (a) Binarized image generated from laser data, (b) skeletonized image with disconnected segments and (c) skeletonized image after linking the segments.

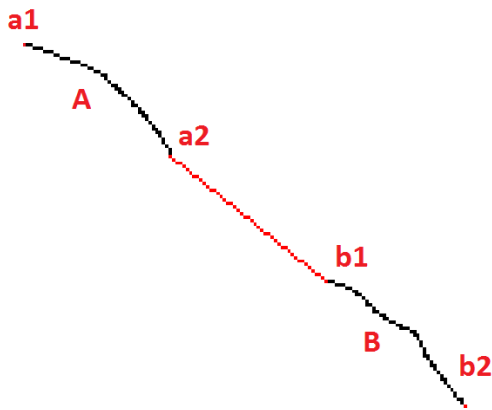


Fig. 20 Example of segments connection.

$$\alpha = \arccos\left(\frac{u \cdot v}{|u| \cdot |v|}\right) \quad (11)$$

In the second step the thresholds for angulation and distance are larger; however is added one more rule, the region between the two points that will be connected should be green. We consider as green the points that satisfy the conditions $(R/G) < 1.12$ and $(B/G) < 1.05$ and $(R+G+B) < 310$, where R, G and B are the red, green and blue components of the RGB system. The condition used above showed to be very effective as shown in Fig. 21.

The color information are stored in the digital image, thus, for this step we need to use the correspondence matrix generated in matching process. Using the correspondence matrix we can find the points P1 and P2 that represent to the points in the laser data that will be connected (extremities of the segments).

After finding the points P1 and P2 in the digital image, we join the pixels between them using the

algorithm of Bresenham (1965). The algorithm of Bresenham determines the pixels that belong to the straight line that links two pixels, as shown in Fig. 22.

Every pixel that belongs to this line has its color verified. The points P1 and P2 are connected when at least 65% of the pixels in the line are green. In Fig. 23 is shown an example of segments connected in this step.

6.1.9 Removal of Small Segments

Some segments are very small. They were generated by noise and do not represent roads. Thus, they need be removed. For this purpose, we compute the size of the segments by the number of pixels that form it. The threshold size for the removal of segments was determined empirically. Some removed segments are shown in Fig. 24.

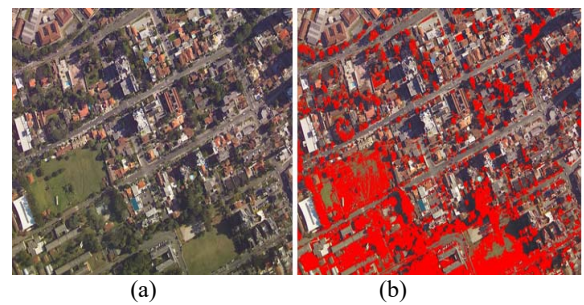


Fig. 21 (a) Original digital image and (b) image with green areas highlighted.

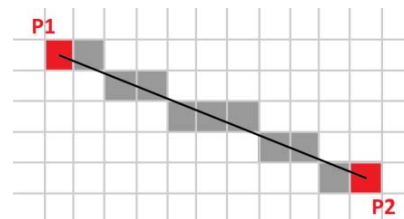


Fig. 22 Points that belong to the straight line that connects P1 and P2 determined by the Bresenham algorithm.

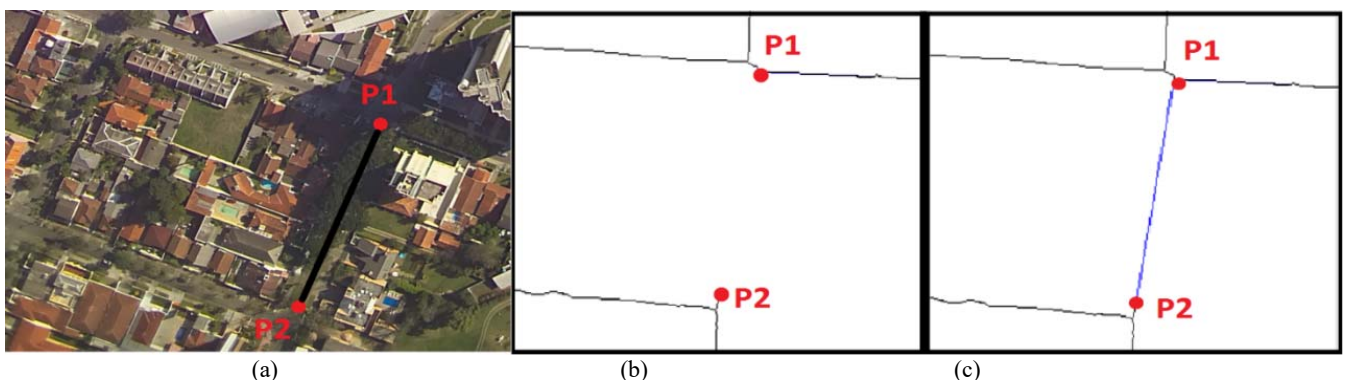


Fig. 23 Example of segments connection performed by the analysis of wooden area. (a) Digital image, (b) points to be connected and (c) the result of the connection process.

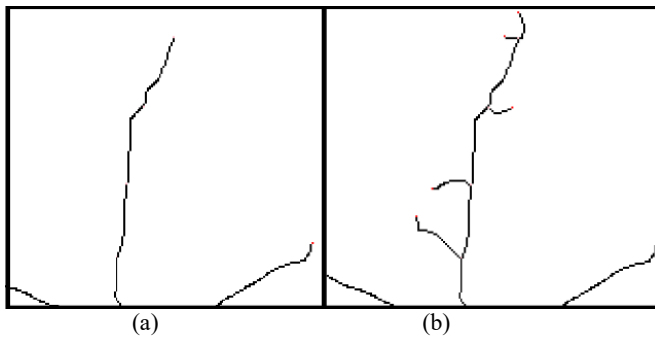


Fig. 24 Example of removal of small segments. (a) Image with small segments to be removed. (b) Resulting image.

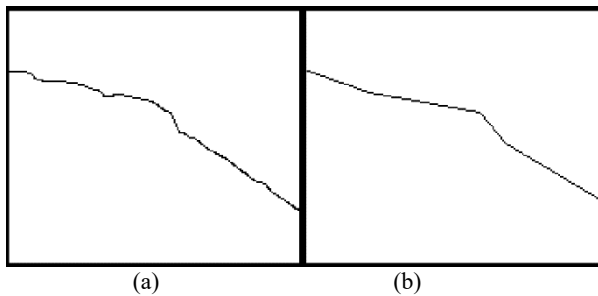


Fig. 25 Example of segment smoothing. (a) Original image. (b) Image with smoothed segments.

6.1.10 Segments Smoothing

The algorithm proposed by Douglas & Peucker (1973) was applied to smooth the obtained lines. The algorithm eliminates points that cause small segments. However, points that represent bigger segments are kept then that most significant curves are preserved.

7 RESULTS

Three sets of laser data and digital images were used of an urban area of the city of Curitiba, state of Parana in Brazil. Each testing set represents a region with overlapping between laser data and the image of a urban area.

In order to analyze the results we manually elaborated templates (Figs 26b, 28b and 30b), based on the laser data e digital images of the three data sets. These templates were used to validate the results obtained after applying the algorithm.

At the end of all processing is generated an image with all detected roads. To validate the results we subtract the resulting image from the template. Then, we were able to count the points that correspond to true positives (urban roads) and false positives (regions wrongly detected). The counting of points corresponding to false negatives (not detected roads) was done by demarcating these points in the resulting image.

Figures 27, 29 and 31 show points that were correctly detected (in black) and points misclassified

(false positive in red and false negative in green) for the first data set. The same process was also applied to the second and third data set.

The numbers of black, red and green pixels were counted for each experiment. The results are shown in Table 2. We also computed the Sensibility S , which measures the capacity to correctly detect urban roads among those that actually exist, and the Positive Predictive Value PPV , which represents the proportion of urban roads correctly detected, as shown in Eqs (12) and (13), respectively:

$$S = TP / (TP + FN) \quad (12)$$

$$PPV = TP / (TP + FP) \quad (13)$$

where TP is the number of True Positive, FN is the number of False Negatives and FP is the number of False Positives.

The results presented show that the algorithm proposed achieved a good sensibility rate, as it correctly detected most of the existing roads in the three experiments. Nevertheless, in the three experiments the Positive Predictive Value show a small rate due to the fact that the algorithm detects besides the asphalt, parking lots and driveways as roads (false positives).

Table 2. Results counting

	Exp. 1	Exp. 2	Exp. 3
True Positives	10 966	12 249	15 174
False Positives	2671	5980	4440
False Negatives	611	1011	1103
Sensibility	94.7%	92.4%	93.2%
Positive Predictive Value	80.4%	67.2%	77.4%

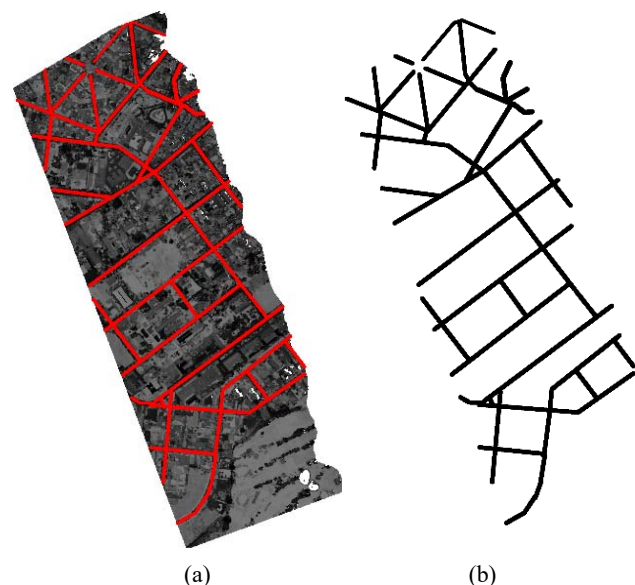


Fig. 26. (a) Laser data and superimposed template. (b) Manually generated template (first data set).

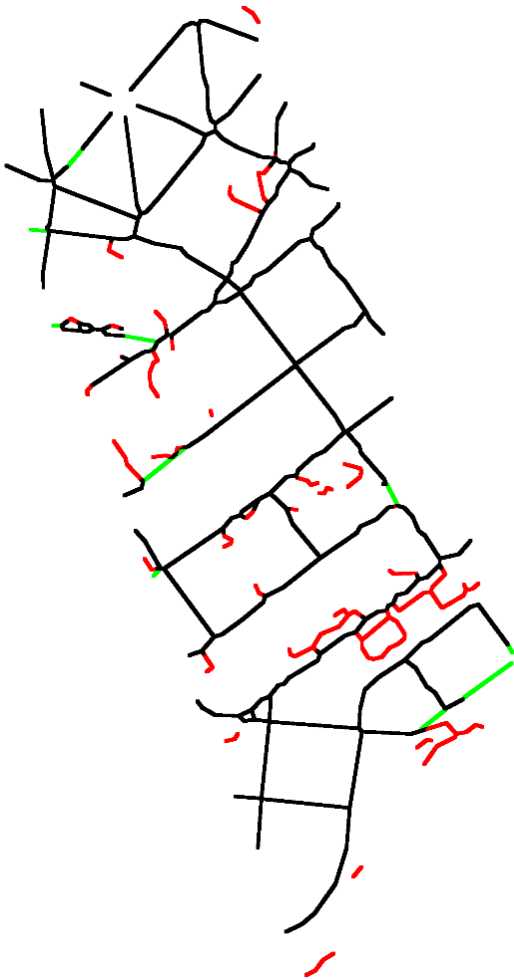


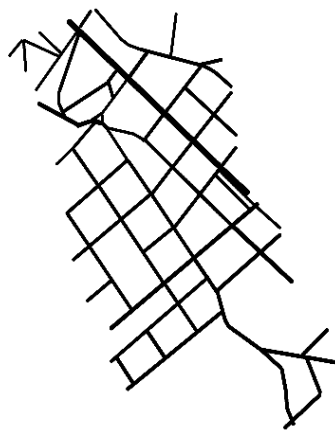
Fig. 27 Image containing mistakes and successes of the algorithm for the first data set (the image, whose lines had width of 1 pixel, was dilated for better viewing).



Fig. 29 Image containing mistakes and successes of the algorithm for the second data set (the image, whose lines had width of 1 pixel, was dilated for better viewing).



(a)

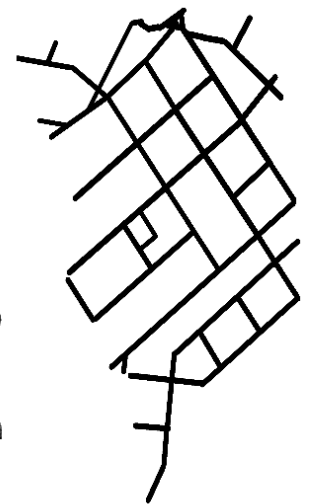


(b)

Fig. 28 (a) Laser data and superimposed template. (b) Manually generated template (second data set).



(a)



(b)

Fig. 30 (a) Laser data and superimposed template. (b) Manually generated template (third data set).



Fig. 31 Image containing mistakes and successes of the algorithm for the third data set (the image, whose lines had width of 1 pixel, was diluted for better viewing).

8 CONCLUSION

The use of intensity of laser pulse response, height and color, were useful for the task of extracting urban roads. Each type of information provided a unique contribution; the merging of them enhanced the final result. Based on the experiments, we noticed that the number of false positives was bigger than the number of false negatives, and in most cases, it happened due to parking areas and driveways. On the other hand, the false negatives occurred, in general, due to road occlusion by trees. However, it is interesting noting that in the regions where a small part of the road was covered by trees, the algorithm was able to detect it.

A main difficult we faced was the use of image with perspective deformities, due to viewing angles of the cameras. This problem affected significantly the areas closer to the boundaries of the image; the matching presented considerably displacements in this region. The use of orthophotos would eliminate this problem; but this type of image was not available for this region.

The results obtained were very satisfactory, mainly due to difficulty and the challenge of this application. The proposed method obtained precision of above the 92%. We expect refine the detection of urban roads using a larger amount of laser data and images from the same area.

REFERENCES

- Alves, F.L.B. (2007) Avaliação da Extração Semiautomática de Rodovias Sobre uma Imagem Híbrida para Atualização Cartográfica. Dissertação de Mestrado em Engenharia Cartográfica, Rio de Janeiro: Instituto Militar de Engenharia.
- Araki, H. (2005) Fusão de informações espectrais, altimétricas e de dados auxiliares na classificação de imagens de alta resolução espacial. Curitiba. Tese de Doutorado em Ciências Geodésicas, Universidade Federal do Paraná, Curitiba.
- Baumgartner, A.; Steger, C.; Mayer, H.; Eckstein, W. & Ebner, H. (1999) Automatic Road Extraction in Rural Areas. In: *The International Archives of the Photogrammetry, Remote Sensing and Spatial Information Sciences*, v. XXXII, 107–112.
- Bresenham, J.E. (1965) Algorithm for Computer Control of a Digital Plotter. IBM, Systems Journal, 4(1), 25–30.
- Castro, F.S.P.; Debiassi, P. & Centeno, J.A.S. (2009) Extração de Estradas em Imagens de Intensidade Laser Utilizando Morfologia Matemática. In: *Simpósio Brasileiro de Sensoriamento Remoto (SBSR)*, XIV, 2009, Natal: INPE 5001–5007.
- Centeno, J.A.S. & Mitshita, E.A. (2007) Laser scanner aerotransportado no estudo de áreas urbanas: A experiência da UFPR. In: *Simpósio Brasileiro de Sensoriamento Remoto*, 13, Anais... Florianópolis, Brasil, 21-26 abril, INPE. 3645-3652.
- Dal Poz, A.P.; Zanin, R.B. & Vale, G.M. (2006) Automated Extraction of Road Network from Medium- and High-resolution Images. Pattern Recognition and Image Analysis, Pleiades Publishing, Inc, 16(2), 239–248.
- Douglas, D. & Peucker, T. (1973) Algorithms for the Reduction of the Number of Points Required to Represent a Digitized Line or its Caricature. The Canadian Cartographer, 10(2), 112–122.
- Fazan, A.J. & Dal Poz, A.P. (2013) Rectilinear building roof contour extraction based on snakes and dynamic programming. ITC J., 25, 1–10.
- Galvanin, E.A.S. & Dal Poz, A.P. (2009) Roof contours recognition using LiDAR data and Markov random field model on graph theory. In: 24th International Cartographic Conference, 2009, Santiago, Chile. In: *24th International Cartographic Conference. Santiago, Chile: International Cartographic Association*, 1, 1–9.
- Hu, X; Tao, C.V. & Hu, Y. (2004) Automatic road extraction from dense urban area by integrated processing of high resolution imagery LIDAR data. In: *International Archives of the Photogrammetry, Remote Sensing and Spatial Information Science*, Istanbul, 35, 320–325.
- Mena, J. B. (2003) State of the Art on Automatic Road Extraction for GIS Update: a Novel Classification. In: *Pattern Recognition Letters*, 24, 3037–3058.
- Mendes, T.S.G., Fazan, A.J. & Poz, A.P.D. (2004) Delineamento de Estradas Vicinais usando Técnicas de Correlação de Imagens. Dissertação de Mestrando, FCT/UNESP. Presidente Prudente, SP.
- Pereira, D.R., Nakamura, R., Pisani, R., Papa, J.P (2015) Land-cover Classification Through Sequential Learning-Based Optimum-Path Forest. Proceedings of International Geoscience and Remote Sensing Symposium.
- Silva, M.A.O. (2003) Detecção e Reconstrução Automática de Junções de Rodovia em Imagens Digitais de Cenas Rurais. Dissertação do Mestrando em Ciências Cartográficas, FCT/UNESP. Presidente Prudente, SP.
- Wutke, J.D. (2006) Métodos Para Avaliação de um Sistema Laser Scanner Terrestre. Curitiba, 86p. Dissertação de Mestrado em Ciências Geodésicas, Universidade Federal do Paraná, Curitiba.
- Zhang, T.Y.; Suen, C.Y. (1984) A Fast Parallel Algorithm for Thinning Digital Patterns. Communications of the ACM. March, 236–239.

Vosselman, G. (2000) Slope Based Filtering of Laser Altimetry Data. *International Archives of Photogrammetry, Remote Sensing and Spatial Information Sciences*, **33**(B3/2), Amsterdam, Netherlands, 935–942.